Spin dephasing in the dipole field around capillaries and cells: Numerical solution

C. H. Ziener,[1] S. Glutsch,[1] P. M. Jakob,[1] and W. R. Bauer[2]
[1]*Julius-Maximilians-Universität Würzburg, Lehrstuhl für Experimentelle Physik 5, Am Hubland, 97074 Würzburg, Germany*
[2]*Julius-Maximilians-Universität Würzburg, Medizinische Klinik und Poliklinik I, Oberdürrbacher Straße 6, 97080 Würzburg, Germany*
(Received 26 May 2009; published 9 October 2009)

We numerically solve the Bloch-Torrey equation by discretizing the differential operators in real space using finite differences. The differential equation is either solved directly in time domain as initial-value problem or in frequency domain as boundary-value problem. Especially the solution in time domain is highly efficient and suitable for arbitrary domains and dimensions. As examples, we calculate the average magnetization and the frequency distribution for capillaries and cells which are idealized as cylinders and spheres, respectively. The solution is compared with the commonly used Gaussian approximation and the strong-collision approximation. While these approximations become exact in limiting cases (small or large diffusion coefficient), they strongly deviate from the numerical solution for intermediate values of the diffusion coefficient.

DOI: 10.1103/PhysRevE.80.046701 PACS number(s): 02.70.Bf, 76.60.Jx, 87.61.Bj

I. INTRODUCTION

In magnetic resonance imaging, cross sections of the analyzed tissue can be obtained by applying an external magnetic field and a radio frequency pulse. The radio frequency pulse excites the spins in the tissue and the relaxation into the equilibrium can be measured in an experiment. The relaxation process is mainly determined by the dephasing of the spins in the analyzed tissue. Microscopic magnetized objects which are embedded in the tissue influence the dephasing and consequently the measured signal. Such objects which are smaller than the resolution of the obtained image are, for example, a blood filled capillary or a cell labeled with magnetic nanoparticles. In the commonly used Krogh model [1], these capillaries and cells are idealized as cylinders and spheres with reflecting boundary conditions.

The dephasing in a local inhomogeneous field is described by the Bloch-Torrey equation [2]. This equation is a partial differential equation with one time and up to three space variables. As the differential operator for the spatial directions in nonhermitian, expansion into eigenfunctions is of limited value and it is hopeless to find an exact solution for the general case [3]. Analytical solutions have been presented only for very special cases which are mainly of academic interest: the Bloch-Torrey equation has been solved analytically for linear and parabolic field gradients [4,5] and this solution can be generalized to the case that the field gradient is time-dependent [6]. However, for the important cases of dipole fields from cylinders and spheres mentioned above, no analytical solution is available.

As an exact solution is not possible in most relevant cases, approximate methods have been developed for the description of the magnetization decay. Most of theses approximations focus on a special diffusion regime. In the motional-narrowing regime the relaxation effect due to the diffusion of spins is much greater than that due to the susceptibility effect of the field inhomogeneities [7]. The opposite limit is the static dephasing regime in which the diffusion of the spins around the magnetized object is neglected [8]. However, in many applications of magnetic resonance imaging the underlying diffusion regime is neither the motional-narrowing regime nor the static dephasing regime but an intermediate regime. Therefore it was necessary the develop models which include both diffusion regimes and which describe the whole dynamic range. Kennan *et al.* used the Gaussian approximation to analyze susceptibility contrast mechanisms in tissues [9]. Another approximation to describe the whole dynamic range is the strong-collision approximation which was used (see Bauer *et al.* [10,11]) to describe the dephasing in the capillary network of the myocardium. With this approximation it was possible to describe the signal decay of the transverse magnetization by a simple exponential decay $\exp(-t/T_2^*)$, where the transverse relaxation time T_2^* could be given in dependence of the properties of the tissue. Later on, the Gaussian approximation and the strong-collision approximation were applied to study the nonexponential character of the signal decay. Sukstanskii and Yablonskiy used the Gaussian approximation to describe the signal formation in the local magnetic field around cylinders and spheres [12,13]. However, it could be shown that the dephasing exhibits a non-Gaussian character [3,14]. The strong-collision approach was used to develop the formalism of the density of states to describe the effects of diffusion around field inhomogeneities [15] and to develop generally valid scaling laws for the transverse relaxation times [16]. Hürlimann focuses on scaling laws and nondimensional solutions to describe susceptibility effects in porous media in terms of effective gradients [17,18]. What is missing is a numerical method to solve the Bloch-Torrey equation which does not rely on simplifications or idealized assumptions and is not restricted to limiting cases.

In this paper, we present numerical method that allows to accurately solve the Bloch-Torrey equation for arbitrary domains, dimensions, and potentials. The method is applied to cylinders and spheres, and the results are compared with the Gaussian approximation and the strong-collision approximation for various values of the diffusion coefficient. In Sec. II, we recover the general theory of spin dephasing in magnetic resonance with particular emphasis on the Krogh model for cylinders and spheres and briefly introduce the Gaussian approximation and the strong-collision approximation. In Sec. III, we describe the discretization of the differ-

ential operators in real space by finite differences and the solution of the Bloch-Torrey equation in time and frequency domain. In Sec. IV, the method is applied to cylinders and spheres and a comparison is made to the Gaussian and the strong-collision approximation. Summary and conclusions are given in Sec. V.

II. GENERAL THEORY

In this section, we introduce the Bloch-Torrey equation and give explicit expressions for the Krogh model in two and three dimensions. Furthermore, we briefly review the Gaussian approximation and the strong-collision approximation.

A. Bloch-Torrey equation

We consider a single object in a homogeneous external magnetic field $\boldsymbol{B}_0=B_0\boldsymbol{e}_z$. The susceptibility difference $\Delta\chi$ between the object and the surrounding medium causes a magnetization inside the object which gives rise to a local magnetic field $\boldsymbol{B}(\boldsymbol{r})$. The surrounding protons ($g=5.585$, $q=+1.6022\times10^{-19}$ As, and $m=1.6726\times10^{-27}$ kg) gyrate with the local Larmor frequency $\omega(\boldsymbol{r})=\gamma B_z(\boldsymbol{r})$, where $\gamma=gq/2m=2.675\times10^{-8}$ $\mathrm{s}^{-1}\,\mathrm{T}^{-1}$ is the gyromagnetic ratio of a proton. It is customary to decompose the local Larmor frequency as

$$\omega(\boldsymbol{r}) = \delta\omega W(\boldsymbol{r}). \tag{1}$$

The frequency shift $\delta\omega$ is proportional to γB_0 and depends on the susceptibility difference, whereas the dimensionless potential $W(\boldsymbol{r})$ is on the order of unity and is solely determined by the geometry of the magnetized object.

The time evolution of the transverse magnetization of spins is governed by the Bloch-Torrey equation [2]

$$\frac{\partial}{\partial t}m(\boldsymbol{r},t) = [D\Delta + \mathrm{i}\,\delta\omega W(\boldsymbol{r})]m(\boldsymbol{r},t), \tag{2}$$

which describes diffusion with diffusion coefficient $D\geq0$ and, at the same time, accumulation of a phase angle due to gyration. In magnetic resonance imaging the measured signal is given by averaging over the dephasing volume [8]

$$M(t) = \frac{1}{G}\int_G dv\, m(\boldsymbol{r},t). \tag{3}$$

The distribution of spins is homogeneous and immediately after the 90° high-frequency pulse at $t=0$, the phase angle of each spin is zero. Thus we have the initial condition

$$m(\boldsymbol{r},0) \equiv 1 \tag{4}$$

and it holds that $M(0)=1$. In addition, reflecting boundary conditions apply for the Krogh model, which will be discussed in the next subsection.

It is convenient, also in view of numerical calculations, to use the Dirac notation with

$$\langle\boldsymbol{r}|\varphi\rangle = \varphi(\boldsymbol{r}); \quad \langle\boldsymbol{r}|\hat{W}|\boldsymbol{r}'\rangle = W(\boldsymbol{r})\,\delta(\boldsymbol{r}-\boldsymbol{r}');$$

$$\langle\varphi|\psi\rangle = \int_G dv\,\varphi^*(\boldsymbol{r})\psi(\boldsymbol{r}). \tag{5}$$

Then the Bloch-Torrey equation (2) writes as

$$\frac{d}{dt}|m(t)\rangle = [D\Delta + \mathrm{i}\,\delta\omega\hat{W}]|m(t)\rangle. \tag{6}$$

Instead of Eqs. (3) and (4), we incorporate the factor $1/G$ in the initial condition,

$$m(\boldsymbol{r},0) = \langle\boldsymbol{r}|0\rangle \equiv \frac{1}{\sqrt{G}}, \tag{7}$$

so that the average magnetization (3) has a symmetric appearance

$$M(t) = \langle m(0)|m(t)\rangle. \tag{8}$$

Importantly, for reflecting boundary conditions (see Sec. II B), the operator $-\Delta$ is hermitian and positive semidefinite. The nondegenerate ground state is given by the expression (7), and the corresponding eigenvalue is zero.

Mathematically, the Bloch-Torrey equation is an initial-value problem (or initial-boundary-value problem) of a partial differential operator. The difficulty, analytically and numerically, lies in the fact that the operator is neither hermitian, as for a Schrödinger equation, nor antihermitian, as for a diffusion equation.

The Fourier transform of the average magnetization is defined as

$$p(\omega) = \frac{1}{2\pi}\int_{-\infty}^{+\infty} dt e^{-\mathrm{i}\omega t}M(t), \tag{9}$$

where the continuation of the signal for negative time arguments is explained as $M(-t)=M^*(t)$. The function p is necessary to describe more sophisticated pulse sequences [19–22]. To derive a compact expression for $p(\omega)$, we consider $|m^+(t)\rangle=\Theta(t)|m(t)\rangle$ which obeys the inhomogeneous differential equation,

$$\frac{d}{dt}|m^+(t)\rangle - [D\Delta + \mathrm{i}\,\delta\omega\hat{W}]|m^+(t)\rangle = \delta(t)|0\rangle,$$

that can be solved by Fourier transform,

$$|\tilde{m}^+(\omega)\rangle = [\mathrm{i}(\omega-\mathrm{i}0^+)\hat{I} - D\Delta - \mathrm{i}\,\delta\omega\hat{W}]^{-1}\frac{1}{2\pi}|0\rangle,$$

where $\hat{I}$ is the identity operator and 0^+ denotes a positive infinitesimal to ensure analyticity on the lower complex half plane. As $p(\omega)=2\,\mathrm{Re}\langle0|\tilde{m}^+(\omega)\rangle$, we obtain

$$p(\omega) = \frac{1}{\pi}\mathrm{Re}\langle0|[\mathrm{i}(\omega-\mathrm{i}0^+)\hat{I} - D\Delta - \mathrm{i}\,\delta\omega\hat{W}]^{-1}|0\rangle. \tag{10}$$

In order to numerically calculate $p(\omega)$ from the above formula, a boundary-value problem has to be solved for each ω.

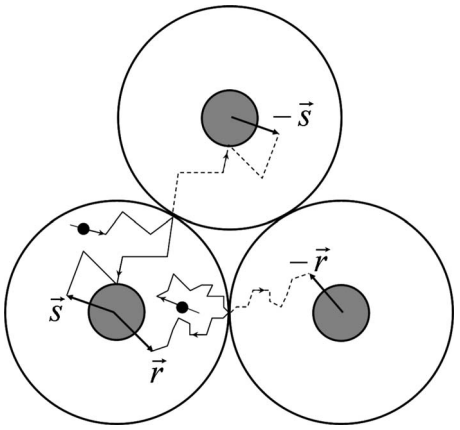

FIG. 1. Cross-sectional view of a set of parallel capillaries and sample trajectories of nuclear spins that leave one supply area and enter the neighboring supply area. The original trajectory is replaced by a trajectory that is reflected at the boundary.

Besides

$$\int_{-\infty}^{+\infty} d\omega p(\omega) = M(0) = 1, \tag{11}$$

the function p has the important property

$$p(\omega) \geq 0. \tag{12}$$

This can be seen from rewriting Eq. (10) as

$$p(\omega) = \frac{1}{\pi}\langle\varphi(\omega)|[-D\Delta + 0^+\hat{I}]|\varphi(\omega)\rangle,$$

where

$$|\varphi(\omega)\rangle = [\mathrm{i}(\omega - \mathrm{i}0^+)\hat{I} - D\Delta - \mathrm{i}\delta\omega\hat{W}]^{-1}|0\rangle,$$

and the positive semidefiniteness of the operator $-\Delta$. Therefore, $p(\omega)$ can be looked upon as probability density of the frequency distribution. In the static case, when $D=0$, by virtue of the Dirac identity, expression (10) goes over into

$$p_0(\omega) = \frac{1}{G}\int_G dv\, \delta[\omega - \delta\omega W(\mathbf{r})], \tag{13}$$

which is the classical density of states.

B. Krogh model

Krogh's capillary model [1] is commonly used in medicine to describe physiological effects in the myocardium. The myocardium of the heart consists of blood-filled capillaries with radius R_1 which are arranged in parallel and form an almost regular structure, see Fig. 1. It is reasonable to assign to each capillary an area of tissue that is predominantly supplied by this capillary. The outer radius is determined such that

$$\eta = \left(\frac{R_1}{R_2}\right)^2, \tag{14}$$

where η is the volume fraction of the blood-filled capillaries. A diffusing particle, which leaves the supply volume of one capillary, enters the supply volume of the neighboring capillary. Exactly the same contribution to the signal would be produced by a particle that is reflected at the outer boundary of the supply volume. During the time period of the dephasing process, exchange of water molecules between the capillary and the surrounding tissue is negligible. Therefore, the diffusion of spins can be modeled by considering coaxial cylinders with radii $R_1 < R_2$ and reflecting boundaries on both surfaces.

We shall now specify the terms of the Bloch-Torrey equation for coaxial cylinders with reflecting boundary conditions. It is useful to employ cylinder coordinates ρ, ϕ, ζ. Because of the translational invariance in the axial (ζ) direction, the problem can be reduced to two dimensions. Then the domain, the volume element, the boundary conditions, and the Laplacian are given by

$$G_{\rho\phi} = \{(\rho,\phi)|R_1 \leq \rho \leq R_2; 0 \leq \phi \leq 2\pi\}; \quad dv = d\phi d\rho\rho$$

$$\frac{\partial m(\rho,\phi,t)}{\partial \rho} = 0 \quad \text{for} \quad \rho = R_1 \quad \text{or} \quad \rho = R_2$$

$$\Delta = \frac{1}{\rho}\frac{\partial}{\partial\rho}\left(\rho\frac{\partial}{\partial\rho}.\right) + \frac{1}{\rho^2}\frac{\partial^2}{\partial\phi^2} = \Delta_\rho + \frac{1}{\rho^2}\Delta_\phi. \tag{15}$$

The local magnetic field is derived in [19]. For a tilt angle ϑ between the cylinders and the external magnetic field, the frequency shift and potential are

$$\delta\omega = \gamma\frac{\Delta\chi}{2}B_0 \sin^2\vartheta; \quad W(\rho,\phi) = \frac{R_1^2}{\rho^2}\cos(2\phi). \tag{16}$$

As $W(\rho, \frac{\pi}{2} - \phi) = -W(\rho,\phi)$, it holds that $m(\rho, \frac{\pi}{2} - \phi) = m^*(\rho,\phi)$ and, therefore, $M(t)$ is real.

If the Bloch-Torrey equation is solved on the domain (15), periodic boundary conditions have to be applied for the coordinate ϕ. As the potential is periodic in the argument ϕ with period π and symmetric around $\phi=0$ and $\phi=\frac{\pi}{2}$, the coordinate ϕ can be restricted to $0 \leq \phi \leq \frac{\pi}{2}$ with reflecting boundary conditions on both ends.

Likewise, the spin diffusion around magnetically labeled cells can be described by a concentric spherically dephasing volume with reflecting boundary conditions. The relation between the radii and the volume fraction is

$$\eta = \left(\frac{R_1}{R_2}\right)^3. \tag{17}$$

In the case of spheres, spherical coordinates $r, \varepsilon = \cos\theta, \phi$ are suitable for the problem. Because the system possesses rotational symmetry around the magnetic field (z) axis, there is no dependence on the angle ϕ and, mathematically, the problem is only two-dimensional. The domain, the volume element, the boundary conditions, and the Laplacian are given by

$$G_{r\varepsilon} = \{(r,\varepsilon)|R_1 \leq r \leq R_2; -1 \leq \varepsilon \leq +1\}; \quad dv = d\varepsilon dr r^2$$

$$\frac{\partial m(r,\varepsilon,t)}{\partial r} = 0 \quad \text{for} \quad r = R_1 \quad \text{or} \quad r = R_2$$

$$\Delta = \frac{1}{r^2}\frac{\partial}{\partial r}\left(r^2\frac{\partial}{\partial r}.\right) + \frac{1}{r^2}\frac{\partial}{\partial \varepsilon}\left[(1-\varepsilon^2)\frac{\partial}{\partial \varepsilon}.\right] = \Delta_r + \frac{1}{r^2}\Delta_\varepsilon. \tag{18}$$

The frequency shift and potential for a magnetic sphere are [19]

$$\delta\omega = \gamma\frac{\chi}{3+\chi}B_0; \quad W(r,\varepsilon) = \frac{R_1^3}{r^3}(3\varepsilon^2-1). \tag{19}$$

This time, the potential is not an odd function of ε and $M(t)$ is complex. As $(1-\varepsilon^2)\partial m/\partial\varepsilon$ vanishes at $\varepsilon=\pm 1$, reflecting boundary conditions apply also for the coordinate ε (cf. Sec. III). Because $W(r,-\varepsilon)=W(r,\varepsilon)$, the coordinate ε can be restricted to $0\le\varepsilon\le 1$ with reflecting boundary conditions on both ends.

C. Gaussian approximation

An equivalent formulation for the average magnetization (8) is [23]

$$M(t_2-t_1) = \langle\langle \Psi^*(t_1)\Psi(t_2)\rangle\rangle;$$

$$\Psi(t) = \exp\left[\mathrm{i}\delta\omega\int_0^t dt'\Omega(t')\right]. \tag{20}$$

Here, $\langle\langle\cdots\rangle\rangle$ denotes the statistical average and

$$\Omega(t) = \omega[\boldsymbol{R}(t)] \tag{21}$$

is a stochastic process, where $\boldsymbol{R}(t)$ is the realization of a random walk with diffusion coefficient D in the domain G subjected to reflecting boundary conditions.

If the stochastic process is assumed to be Gaussian which is adequate in the motional-narrowing regime and for short times [24], then, as shown by Anderson and Weiss [25], M is entirely determined by the two-point correlation function and it holds that

$$M(t) = \exp\left[-\int_0^t dt'\int_0^{t'} dt''K(t'')\right];$$

$$K(t_2-t_1) = \langle\langle\Omega(t_1)\Omega(t_2)\rangle\rangle. \tag{22}$$

The Gaussian approximation considerably simplifies the calculation, as the two-point correlation function follows from a diffusion equation [26,27]

$$K(t) = (\delta\omega)^2 L(|t|)$$

$$L(t) = \langle w(0)|w(t)\rangle \quad \text{for} \quad t\ge 0; \quad L(-t) = L(t)$$

$$\frac{d}{dt}|w(t)\rangle = D\Delta|w(t)\rangle; \quad \langle \boldsymbol{r}|w(0)\rangle = \frac{W(\boldsymbol{r})}{\sqrt{G}}, \tag{23}$$

with reflecting boundary conditions for $w(\boldsymbol{r},t)$ which is much easier to solve than the original Bloch-Torrey equation. Importantly, as $L(t)$ is real, the average magnetization in Gaussian approximation is always real.

Instead of solving a diffusion equation in time domain, L can be expressed by the eigenvalues k_n^2 and eigenstates $|n\rangle$ of the operator $-\Delta$ according to

$$L(t) = \sum_{n=0}^{\infty} \mathrm{e}^{-k_n^2 D|t|}|\langle n|w(0)\rangle|^2; \quad 0 = k_1^2 < k_2^2 \le \cdots \le k_n^2. \tag{24}$$

For cylinders and spheres, the calculation of L reduces to an eigenvalue problem of an ordinary differential operator [28]. Because of $\langle 0|w(0)\rangle = 0$, the term with $n=0$ does not contribute to the sum. Therefore, it holds that $L(t)\to 0$ as $D|t|\to\infty$ and for large values of $D|t|$, the average magnetization shows a linear exponential decay.

The solution in Gaussian approximation could be simplified further by changing to the variable $u=Dt$. Then, after L as function of u was calculated once for a geometry under consideration, $M(t)$ would be known for each D and $\delta\omega$.

For $D=0$ it holds that $L(t)\equiv L(0)=\langle w(0)|w(0)\rangle$ and the average magnetization and frequency distribution are known analytically:

$$M_0(t) = \mathrm{e}^{-1/2(\delta\omega)^2 L(0)t^2}$$

$$p_0(\omega) = \frac{\exp\left[-\dfrac{\omega^2}{2(\delta\omega)^2 L(0)}\right]}{\sqrt{2\pi(\delta\omega)^2 L(0)}}. \tag{25}$$

Thus, for $D=0$, the frequency distribution is always a Gaussian, independent of the particular form of the potential W, and the width of the distribution, characterized by the second moment, is the same as for the classical density of states (13). This shows a principal limitation of the Gaussian approximation.

From the explicit expressions (16) and (19) it follows that:

$$L(0) = \frac{1}{2}\left(\frac{R_1}{R_2}\right)^2 = \frac{1}{2}\eta \tag{26}$$

in the case of cylinders and

$$L(0) = \frac{4}{5}\left(\frac{R_1}{R_2}\right)^3 = \frac{4}{5}\eta \tag{27}$$

in the case of spheres.

In the representation (20), the magnetization fulfills $M(0)=1$ and, by virtue of the Wiener-Khintchine theorem, its Fourier transform which is the spectral function of the stochastic process is nonnegative. In the Gaussian approximation, an assumption is made only on the stochastic process (21), while the general representation (20) remains unchanged. In fact, as already noticed by Anderson and Weiss [25], it is possible to generate a Gaussian stochastic process for a given autocorrelation function, e.g., for expression (24). Therefore, also in the Gaussian approximation $p(\omega)$ has the properties of a probability density.

D. Strong-collision approximation

In the strong-collision approximation, the frequency distribution is approximated as [15]

$$p(\omega) = \frac{1}{\pi}\mathrm{Re}\left\{\left\{\frac{1}{G}\int_G \frac{dv}{\frac{1}{\tau} + \mathrm{i}[\omega - \delta\omega W(\boldsymbol{r})]}\right\}^{-1} - \frac{1}{\tau}\right\}^{-1}, \tag{28}$$

where the correlation time is given by [29]

$$\tau = \frac{\langle u|w\rangle}{\langle w|w\rangle} \tag{29}$$

and $u(\boldsymbol{r})$ is the solution of the boundary-value problem

$$-D\Delta|u\rangle = |w\rangle \tag{30}$$

with reflecting boundary conditions. The approximate result (28) is equivalent to replacing the operator $-D\Delta$ in Eq. (10) by $(\hat{I} - |0\rangle\langle 0|)/\tau$. Therefore, the relations (11–12) are also fulfilled in the strong-collision approximation. In essence, the function (28) equals the density of states (13), subjected to a lifetime broadening of width $1/\tau$.

In a recent work [15], we evaluated Eq. (28) for cylinders and spheres yielding

$$p(\omega) = \frac{\tau}{\pi}\mathrm{Re}\frac{H\left(\frac{1+\mathrm{i}\tau\omega}{\eta\tau\delta\omega}\right) - \eta H\left(\frac{1+\mathrm{i}\tau\omega}{\tau\delta\omega}\right)}{(1-\eta)(1+\mathrm{i}\tau\omega) - H\left(\frac{1+\mathrm{i}\tau\omega}{\eta\tau\delta\omega}\right) + \eta H\left(\frac{1+\mathrm{i}\tau\omega}{\tau\delta\omega}\right)}, \tag{31}$$

with the correlation time

$$\tau = \frac{R_1^2}{D}k(\eta).$$

The functions H and k take the form

$$H(x) = \sqrt{1 + \frac{1}{x^2}}; \quad k(\eta) = \frac{1}{4}\frac{\ln\,\eta}{\eta - 1}$$

for cylinders and

$$H(x) = \frac{1}{3} + \frac{2}{3}\sqrt{\frac{1-\mathrm{i}x}{3}}\left(1 - \frac{2\mathrm{i}}{x}\right)\mathrm{arccoth}\left(\sqrt{\frac{1-\mathrm{i}x}{3}}\right);$$

$$k(\eta) = \frac{1}{2(1-\eta)}\left[1 - \eta^{1/3} + \frac{4(1-\eta)^2 + 9(2\eta - \eta^{5/3} - \eta^{1/3})}{36(\eta^{5/3} - 1)}\right]$$

for spheres.

III. NUMERICAL SOLUTION

In this section we derive discretization schemes in space and time for the numerical solution of the diffusion equation (23), the Bloch-Torrey equation in time domain (6), and in frequency domain (10) for the geometries introduced in Sec. II B.

We mention that the numerical method is not restricted to these particular cases; numerical solutions can be obtained for arbitrary domains and boundary conditions. For example, one could study the validity of the Krogh model by solving the Bloch-Torrey equation for a periodic array of cylinders or spheres. Furthermore, other kinds of boundary conditions, e.g., relaxing or permeable boundary conditions, discussed in the context of the Bloch-Torrey equation [3], can be incorporated.

The discretization of the Laplacian in Cartesian coordinates is straightforward, and recipes can be found in the literature (see, e.g., [30,31]). This would be the method of choice for irregular domains. However, for the domains under consideration (15, 18), it is favorable to employ plane polar or spherical coordinates, respectively, which is more efficient, but also more theoretically demanding.

For the numerical solution, it is convenient to change to dimensionless quantities. We set $R_1 = D + R_1^2\delta\omega = 1$, i.e., lengths and times are given in units of R_1 and $R_1^2/(D + R_1^2\delta\omega)$, respectively. This choice is preferable over $R_1 = D = 1$ or $R_1 = \delta\omega = 1$ which are not applicable in both limits $D = 0$ and $\delta\omega = 0$.

A. Discretization in real space

In order to numerically solve the initial-value problems (23,6) or the boundary-value problem (10), the Dirac vectors and operators are converted into vectors and matrices. A major advantage of the discretization in real space is the fact that local potentials and differential operators result in sparse matrices where the number of nonzero matrix elements scales linearly with the matrix dimension. The method of finite differences is explained in a number of textbooks, e.g., [32,33].

A state $|\varphi\rangle$ is represented by an n-dimensional vector $\boldsymbol{\varphi}$ of function values at discrete points $\boldsymbol{r}_k$

$$\boldsymbol{\varphi} = (\varphi_k)_{k=1,\ldots,n}; \quad \varphi_k = \varphi(\boldsymbol{r}_k); \quad k = 1, \ldots, n. \tag{32}$$

Here, we shall only give explicit expressions for cylinder coordinates; the derivation for spherical coordinates is completely analogous.

To preserve the rectangular structure of the domain and the orthogonality of the curvilinear coordinates, we define a grid as a product of equally spaced one-dimensional grids according to

$$\rho_i = R_1 + (i-1)h_\rho; \quad i = 1, \ldots, n_\rho; \quad h_\rho = \frac{R_2 - R_1}{n_\rho - 1}$$

$$\phi_j = (j-1)h_\phi; \quad j = 1, \ldots, n_\phi; \quad h_\phi = \frac{\pi/2}{n_\phi - 1}$$

$$\boldsymbol{r}_k = (\rho_i, \phi_j); \quad k = (i-1)n_\phi + j; \quad k = 1, \ldots, n; \quad n = n_\rho n_\phi. \tag{33}$$

Here, h_ρ and h_ϕ are the mesh sizes and n_ρ and n_ϕ are the number of mesh points for the ρ and ϕ direction, respectively. We already took into account the symmetry condition at $\phi = \pi/2$ and restricted the ϕ interval to $[0, \pi/2]$.

The scalar product (5) with the volume element (15) [or Eq. (18), respectively] is approximated as

$$\langle \varphi | \psi \rangle = \boldsymbol{\varphi}^{\dagger} h \boldsymbol{G} \boldsymbol{\psi}, \tag{34}$$

where the superscript † denotes the hermitian conjugate, $h=h_\rho h_\phi$, and the diagonal matrix $\boldsymbol{G}$ contains the weights for the numerical integration by the trapezoidal rule

$$\boldsymbol{G} = (g_{kk'})_{k,k'=1,\ldots,n}; \quad g_{kk'} = \delta_{ii'}\delta_{jj'} g_{\rho,i} g_{\phi,j}$$

$$g_{\rho,i} = \begin{cases} \rho_i & \text{for } i = 2, \ldots, n_\rho - 1 \\ \frac{1}{2}\rho_i & \text{for } i = 1, n_\rho \end{cases}$$

$$g_{\phi,j} = \begin{cases} 1 & \text{for } j = 2, \ldots, n_\phi - 1 \\ \frac{1}{2} & \text{for } j = 1, n_\phi. \end{cases} \tag{35}$$

Importantly, the weights are products of weights for the individual directions.

In the formalism introduced, the equation $|\psi\rangle = \hat{A}|\varphi\rangle$ translates into $\boldsymbol{\psi}=\boldsymbol{A}\boldsymbol{\varphi}$, where $\boldsymbol{A}$ is the matrix representation of the operator $\hat{A}$. The conversion of the local potential $\hat{W}$ into a matrix is straightforward and leads to a diagonal matrix

$$\boldsymbol{W} = (W_{kk'})_{k,k'=1,\ldots,n}; \quad W_{kk'} = \delta_{kk'} W(\boldsymbol{r}_k). \tag{36}$$

The matrix representation of the Laplacian (15) [or Eq. (18), respectively] can be decomposed as

$$\boldsymbol{\Delta} = (\Delta_{kk'})_{k,k'=1,\ldots,n}; \quad \Delta_{kk'} = \Delta_{\rho,ii'}\delta_{jj'} + \delta_{ii'}\frac{1}{\rho_i^2}\Delta_{\phi,jj'}. \tag{37}$$

The remaining task is to find the discretization of the one-dimensional Laplacians Δ_ρ and Δ_ϕ (15) [or Δ_r and Δ_ε (18), respectively]. For this purpose, we consider a scalar variable λ in a one-dimensional domain $[\Lambda_1, \Lambda_2]$ with a scalar product

$$\langle \varphi | \psi \rangle = \int_{\Lambda_1}^{\Lambda_2} d\lambda g(\lambda) \varphi^*(\lambda) \psi(\lambda); \quad g(\lambda) > 0$$

for

$$\lambda \in [\Lambda_1, \Lambda_2], \tag{38}$$

a general Laplacian of the form

$$\Delta = \frac{1}{g(\lambda)} \frac{d}{d\lambda} \left[k(\lambda) \frac{d}{d\lambda} \cdot \right]; \quad k(\lambda) > 0 \quad \text{for} \quad \lambda \in (\Lambda_1, \Lambda_2), \tag{39}$$

and reflecting boundary conditions

$$k(\lambda)\varphi'(\lambda) = 0 \quad \text{for} \quad \lambda = \Lambda_1 \quad \text{or} \quad \lambda = \Lambda_2 \tag{40}$$

for the functions under consideration. It is important to note that a reflecting boundary condition can also mean that $k(\lambda)=0$ as for spherical coordinates (18) at $\varepsilon = \pm 1$.

The general Laplacian with reflecting boundary conditions has the important properties

$$\langle \varphi | -\Delta \psi \rangle = \int_{\Lambda_1}^{\Lambda_2} d\lambda k(\lambda) \varphi'^*(\lambda) \psi'(\lambda) = \langle -\Delta \varphi | \psi \rangle;$$

$$\int_{\Lambda_1}^{\Lambda_2} d\lambda g(\lambda) \Delta\varphi(\lambda) = 0. \tag{41}$$

The first line is known as hermiticity and the second line can be interpreted as conservation of the number of particles. Furthermore, it holds that

$$\langle \varphi | -\Delta \varphi \rangle = \int_{\Lambda_1}^{\Lambda_2} d\lambda k(\lambda) |\varphi'(\lambda)|^2 \geq 0$$

$$\Delta\varphi(\lambda) = 0 \quad \text{if and only if} \quad \varphi(\lambda) = \text{const}. \tag{42}$$

This means that $-\Delta$ is positive semidefinite and that the ground state is nondegenerate and given by a constant function.

Suppose the interval $[\Lambda_1, \Lambda_2]$ is represented by a uniform mesh

$$\lambda_i = \Lambda_1 + (i-1)h; \quad i = 1, \ldots, n; \quad h = \frac{\Lambda_2 - \Lambda_1}{n-1} \tag{43}$$

and the scalar product and the particle number are approximated by the trapezoidal rule

$$\langle \varphi | \psi \rangle = h \sum_{i=1}^{n} g_i \varphi_i^* \psi_i$$

$$\int_{\Lambda_1}^{\Lambda_2} d\lambda g(\lambda) \varphi(\lambda) = h \sum_{i=1}^{n} g_i \varphi_i$$

$$g_i = \begin{cases} \frac{1}{2} g(\lambda_i) & \text{for } i = 1, n \\ g(\lambda_i) & \text{for } i = 2, \ldots, n-1. \end{cases} \tag{44}$$

Then the properties (41) and (42) of the general Laplacian translate to

$$g_i \Delta_{ij} = \Delta_{ji}^* g_j$$

$$\sum_i g_i \Delta_{ij} = 0 \tag{45}$$

and

$$-\sum_{i,j} g_i \varphi_i^* \Delta_{ij} \varphi_j \geq 0$$

$$\sum_j \Delta_{ij} \varphi_j = 0 \quad \text{if and only if} \quad \varphi_1 = \cdots = \varphi_n \tag{46}$$

for the matrix representation $\boldsymbol{\Delta} = (\Delta_{ij})_{i,j=1,\ldots,n}$.

To determine the matrix elements Δ_{ij} we use a second-order difference scheme, which yields

$$(\Delta\varphi)_i = \frac{1}{g(\lambda_i)} \frac{k_{i+1/2}\varphi'(\lambda_{i+1/2}) - k_{i-1/2}\varphi'(\lambda_{i-1/2})}{h}$$

$$\varphi'(\lambda_{i+1/2}) = \frac{\varphi(\lambda_{i+1}) - \varphi(\lambda_i)}{h}; \quad \varphi'(\lambda_{i-1/2}) = \frac{\varphi(\lambda_i) - \varphi(\lambda_{i-1})}{h}$$

$$(\Delta\varphi)_i = \frac{1}{g_i}\frac{k_{i-1/2}\varphi_{i-1} - (k_{i-1/2}+k_{i+1/2})\varphi_i + k_{i+1/2}\varphi_{i+1}}{h^2}$$

for the inner points $i=2,\ldots,n-1$. Here, $k_{i\pm1/2}=k(\lambda_{i\pm1/2})$ and the $\lambda_{i\pm1/2}$ are defined in the same way as the λ_i. As result, the one-dimensional Laplacian is represented by a tridiagonal Matrix $\boldsymbol{\Delta}$ whose nonvanishing elements in the rows 2 to $n-1$ are given as

$$\Delta_{i,i-1} = \frac{1}{g_i}\frac{k_{i-1/2}}{h^2}; \quad \Delta_{ii} = -\frac{1}{g_i}\frac{k_{i-1/2}+k_{i+1/2}}{h^2};$$

$$\Delta_{i,i+1} = \frac{1}{g_i}\frac{k_{i+1/2}}{h^2}; \quad i=2,\ldots,n-1. \tag{47}$$

Now we employ the conditions (45) to determine the remaining matrix elements leading to

$$\Delta_{11} = -\frac{1}{g_1}\frac{k_{1.5}}{h^2}; \quad \Delta_{12} = \frac{1}{g_1}\frac{k_{1.5}}{h^2};$$

$$\Delta_{n,n-1} = \frac{1}{g_n}\frac{k_{n-1/2}}{h^2};$$

$$\Delta_{nn} = -\frac{1}{g_n}\frac{k_{n-1/2}}{h^2}. \tag{48}$$

Formally, the expressions are the same as for the inner points (47) if we define $k_{-1/2}=k_{n+1/2}=0$.

The resulting difference scheme is consistent, i.e., in the limit $h\to 0$, the approximation $(\Delta\varphi)_i$ approaches the exact value $\Delta\varphi(\lambda_i)$. Furthermore, the conditions (45) and (46) are fulfilled also for finite step size. This can be seen from the explicit expressions of the Δ_{ij} and from

$$-\sum_{i,j} g_i\varphi_i^*\Delta_{ij}\varphi_j = \sum_{i=2}^{n} k_{i-1/2}\left|\frac{\varphi_i-\varphi_{i-1}}{h}\right|^2.$$

Even though the ground state of the matrix $-\boldsymbol{\Delta}$ is known analytically, it is a good idea to numerically verify that the lowest eigenvalue is zero with sufficient accuracy in order to prevent numerical instabilities or spurious solutions. The eigenvalue problem

$$-\boldsymbol{\Delta}\boldsymbol{\varphi}^{(l)} = E^{(l)}\boldsymbol{\varphi}^{(l)}; \quad l=0,\ldots,n-1; \quad E^{(0)} \le \cdots \le E^{(n-1)} \tag{49}$$

for the nonsymmetric matrix $-\boldsymbol{\Delta}$ is not ideally suited for numerical computation. Multiplication from the left with $\boldsymbol{G}$ leads to the generalized eigenvalue problem

$$-\boldsymbol{G}\boldsymbol{\Delta}\boldsymbol{\varphi}^{(l)} = E^{(l)}\boldsymbol{G}\boldsymbol{\varphi}^{(l)}; \quad \boldsymbol{\varphi}^{(l)\dagger}\boldsymbol{G}\boldsymbol{\varphi}^{(l')} = \delta_{ll'}$$

with $-\boldsymbol{G}\boldsymbol{\Delta}$ symmetric and $\boldsymbol{G}$ symmetric and positive definite, for which standard procedures are readily available. As $\boldsymbol{G}$ is diagonal, the problem can be simplified further by introducing $\boldsymbol{G}^{\pm1/2}=\mathrm{diag}(g_1^{\pm1/2},\ldots,g_n^{\pm1/2})$ and substituting $\boldsymbol{\psi}^{(l)}=\boldsymbol{G}^{1/2}\boldsymbol{\varphi}^{(l)}$. Then the equation

$$-\boldsymbol{G}^{+1/2}\boldsymbol{\Delta}\boldsymbol{G}^{-1/2}\boldsymbol{\psi}^{(l)} = E^{(l)}\boldsymbol{\psi}^{(l)}; \quad \boldsymbol{\psi}^{(l)\dagger}\boldsymbol{\psi}^{(l')} = \delta_{ll'} \tag{50}$$

is an ordinary eigenvalue problem for the symmetric tridiagonal matrix $-\boldsymbol{G}^{+1/2}\boldsymbol{\Delta}\boldsymbol{G}^{-1/2}$, perfectly suited for numerical computation.

B. Solution of the diffusion equation

In the Gaussian approximation, the diffusion equation (23) has to be solved numerically. The solution of the diffusion equation (or, equivalently, the heat-flow equation) is quite simple and is described in a number of textbooks, e.g., in [32,33].

According to the results from the last Subsection, Eq. (23) goes over into

$$\frac{d}{dt}\boldsymbol{w}(t) = D\boldsymbol{\Delta}\boldsymbol{w}(t) \tag{51}$$

and the solution is easily performed using the explicit Euler scheme,

$$\boldsymbol{w}(t+h_t) = \boldsymbol{w}(t) + h_t D\boldsymbol{\Delta}\boldsymbol{w}(t). \tag{52}$$

As the matrix $\boldsymbol{\Delta}$ is sparse, only $O(n)$ floating-point operations are required per time step.

The propagation scheme (52) is stable if the stability criterion

$$h_t \le \frac{2}{D\|\boldsymbol{\Delta}\|} \tag{53}$$

is fulfilled. The spectral norm of $\boldsymbol{\Delta}$ which is the largest eigenvalue in magnitude is given by

$$\|\boldsymbol{\Delta}\| = \|\boldsymbol{\Delta}_\rho\| + \frac{1}{R_1^2}\|\boldsymbol{\Delta}_\phi\| \tag{54}$$

and $\|\boldsymbol{\Delta}_\rho\|$ and $\|\boldsymbol{\Delta}_\phi\|$ can be evaluated numerically solving Eq. (50). To be on the safe side, we choose

$$h_t = 0.9\times\frac{2}{D\|\boldsymbol{\Delta}\|}. \tag{55}$$

Consistency of the difference scheme and stability entails that the numerical solution approaches the exact solution as the mesh size in space goes to zero. Thus, besides a sufficiently fine mesh, no further care is necessary to ensure accuracy of the solution.

From the solution $\boldsymbol{w}(t)$ it is straightforward to calculate the two-point correlation function by $L(t)=\boldsymbol{w}^\dagger(t)h\boldsymbol{G}\boldsymbol{w}(t)$. In order to reduce errors induced by the numerical integration, instead of Eq. (23), we choose the initial condition

$$w_k(0) = \mathrm{const}\times W_{kk},$$

where the constant is chosen such that

$$\boldsymbol{w}^\dagger(0)h\boldsymbol{G}\boldsymbol{w}(0) = L(0)$$

with the exact values of $L(0)$ from Eq. (26) [or Eq. (27), respectively]. For spheres, $\langle 0|w(0)\rangle=0$ is not strictly fulfilled when the integral is calculated by the trapezoidal rule. Therefore, we replace the potential (19) by

TABLE I. Physical and numerical parameters. For cylinders, $(n_1,n_2)=(n_\rho,n_\phi)$; for spheres, $(n_1,n_2)=(n_r,n_\varepsilon)$.

Dim.	R_1 (μm)	R_2 (μm)	D (μm^2/ms)	$\delta\omega$ (1/s)	n_1	n_2
2	5	11.18	0	1000	1281	1601
2	5	11.18	1	1000	41	51
2	5	11.18	2	1000	41	51
2	5	11.18	5	1000	41	51
2	5	11.18	10	1000	41	51
3	5	8.55	0	1000	1281	1601
3	5	8.55	1	1000	41	51
3	5	8.55	2	1000	41	51
3	5	8.55	5	1000	41	51
3	5	8.55	10	1000	41	51

$$W_{kk} = \frac{R_1^3}{r_i^3}(c3\varepsilon_j^2 - 1),$$

where c is close to unity, and is adjusted such that $\boldsymbol{u}^\dagger h\boldsymbol{G}\boldsymbol{w}(0)=0$ with $u_k=1$ for each k.

C. Solution of the Bloch-Torrey equation in time domain

The Bloch-Torrey equation (6) corresponds to the matrix-vector equation

$$\frac{d}{dt}\boldsymbol{m}(t) = (D\boldsymbol{\Delta} + \mathrm{i}\delta\omega\boldsymbol{W})\boldsymbol{m}(t). \tag{56}$$

To obtain an explicit scheme, we modify the Euler step (52) as follows:

$$\boldsymbol{m}(t+h_t) = \mathrm{e}^{1/2\mathrm{i}h_t\delta\omega\boldsymbol{W}}(\boldsymbol{I} + h_t D\boldsymbol{\Delta})\mathrm{e}^{1/2\mathrm{i}h_t\delta\omega\boldsymbol{W}}\boldsymbol{m}(t), \tag{57}$$

where $\boldsymbol{I}$ denotes the identity matrix. As the matrix $\boldsymbol{W}$ is diagonal [see Eq. (36)], its exponential is also diagonal and only $O(n)$ floating-point operations are required per time step.

This time, stability alone is not sufficient, as numerical errors also result from the noncommutativity of the matrices $\boldsymbol{W}$ and $\boldsymbol{\Delta}$. Therefore, instead of Eq. (55), we use a smaller time step

$$h_t = \frac{1}{\dfrac{D\|\boldsymbol{\Delta}\|}{0.9\times 2} + \dfrac{\delta\omega\|\boldsymbol{W}\|}{\epsilon}}, \tag{58}$$

where $\|\boldsymbol{W}\|=\max_k|W_{kk}|$ and the small positive dimensionless parameter ϵ is determined experimentally.

From the solution $\boldsymbol{m}$ the average magnetization is calculated as $M(t)=\boldsymbol{m}^\dagger(0)h\boldsymbol{G}\boldsymbol{m}(t)$. To reduce errors from the numerical integration, instead of directly discretizing the initial state (7), we assign

$$m_k(0) = \text{const}$$

and the constant is chosen such that

$$\boldsymbol{m}^\dagger(0)h\boldsymbol{G}\boldsymbol{m}(0) = M(0) = 1.$$

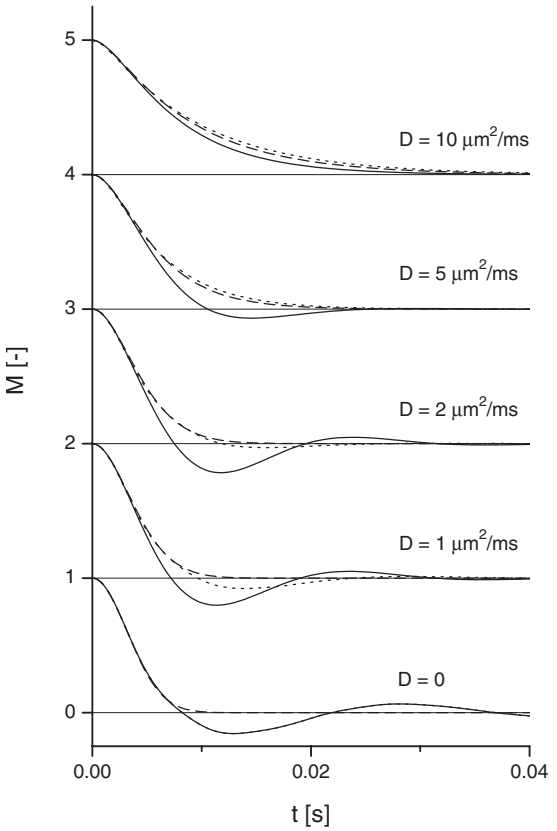

FIG. 2. Average magnetization $M(t)$ in the case of cylinders for $R_1=5$ μm, $R_2=11.18$ μm, $\delta\omega=1000$ s^{-1}, and various values of the diffusion coefficient $D=0$, 1, 2, 5, and 10 μm^2/ms (from bottom to top). Solid line: full numerical solution, dashed line: Gaussian approximation, and dotted line: strong-collision approximation.

D. Solution of the Bloch-Torrey equation in frequency domain

In the finite-difference scheme the expression for the frequency distribution (10) translates into

$$p(\omega) = \frac{1}{\pi}\mathrm{Re}\{h\boldsymbol{m}^\dagger(0)\boldsymbol{G}[\mathrm{i}(\omega - \mathrm{i}0^+)\boldsymbol{I} - D\boldsymbol{\Delta} - \mathrm{i}\delta\omega\boldsymbol{W}]^{-1}\boldsymbol{m}(0)\}. \tag{59}$$

The application of an inverse matrix is equivalent to solving a set of linear equations, which has to be performed for each frequency ω. As the matrix has a finite bandwidth, $2n_\phi+1$ for the arrangement of indices (33), solution by direct methods for matrices with limited bandwidth is feasible. Iterative methods for irregularly sparse matrices, commonly used in the solution of partial differential equations, could be more efficient, but are much more difficult to use.

For $D>0$, the matrix $\mathrm{i}\omega\boldsymbol{I} - D\boldsymbol{\Delta} - \mathrm{i}\delta\omega\boldsymbol{W}$ is regular for each ω and the positive infinitesimal is dropped. For $D=0$, the positive infinitesimal 0^+ has to be replaced by a finite value $\gamma>0$ which plays the role of the inverse lifetime and results in a Lorentzian broadening of the density of states. In this case, the coefficient matrix is diagonal and the finite-difference solution is known explicitly and given by a sum of Lorentzians. The numerical solution for $D=0$ is not of much

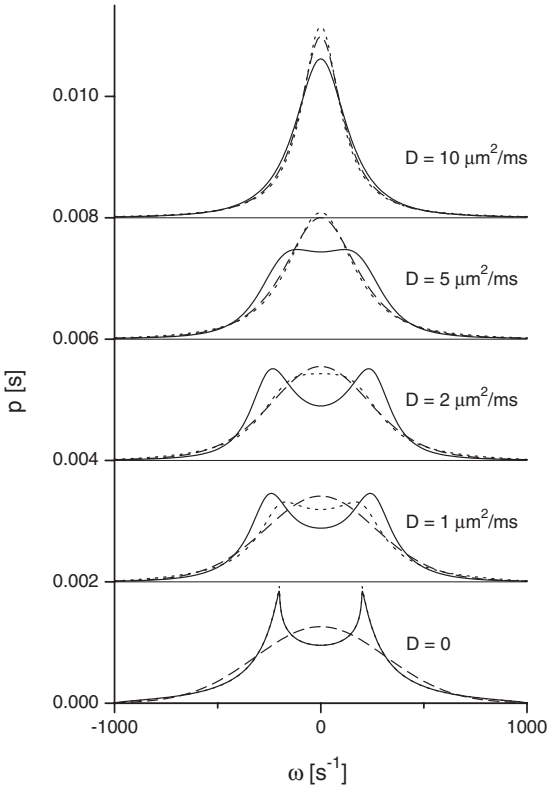

FIG. 3. Frequency distribution $p(\omega)$ in the case of cylinders for $R_1=5$ μm, $R_2=11.18$ μm, $\delta\omega=1000$ s^{-1}, and various values of the diffusion coefficient $D=0$, 1, 2, 5, and 10 μm^2/ms (from bottom to top). Solid line: full numerical solution, dashed line: Gaussian approximation, and dotted line: strong-collision approximation.

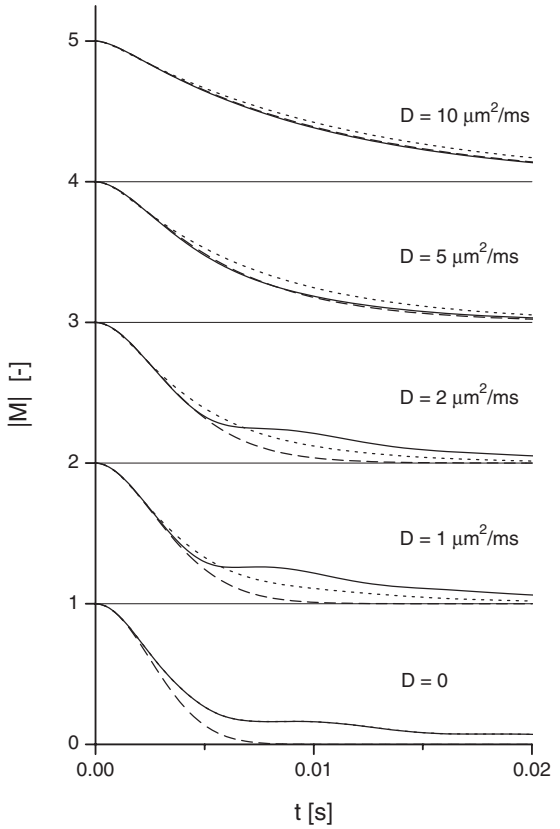

FIG. 4. Average magnetization $|M(t)|$ in the case of spheres for $R_1=5$ μm, $R_2=8.55$ μm, $\delta\omega=1000$ s^{-1}, and various values of the diffusion coefficient $D=0$, 1, 2, 5, and 10 μm^2/ms (from bottom to top). Solid line: full numerical solution, dashed line: Gaussian approximation, and dotted line: strong-collision approximation.

practical interest. However, comparing the numerical solution for $D=0$ with an analytical solution or a solution from a different numerical method is helpful for checking for convergence with respect to the mesh size.

IV. RESULTS

The average magnetization and the frequency distribution were calculated numerically for cylinders and spheres by solving the Bloch-Torrey equation both in time domain and in frequency domain as explained in Secs. III C and III D, respectively. We numerically verified that the solutions of the initial-value problem and the boundary-value problem are equivalent by Fourier transform. For $D>0$, solution in time domain was generally faster. As no field indices have to be reordered, it is also much easier to use and, therefore, the preferred method. A numerical solution of the Bloch-Torrey equation for $D=0$ is not of practical interest, but was performed to make a comparison to the exact solution.

The average magnetization and the frequency distribution were also calculated in the Gaussian approximation. The numerical solution of the diffusion equation according to Sec. III B was much faster than of the original Bloch-Torrey equation, as no Schrödinger term was involved and the time step could be chosen as the maximum possible value allowed by the stability criterion (55). For $D=0$, there is nothing to do, as $w(\boldsymbol{r},t)\equiv w(\boldsymbol{r},0)$ and the solution is known analytically [see Eq. (25)]. Nevertheless, we performed a full numerical solution also for this case to check the accuracy of the numerical time integration in Eq. (22). Furthermore, we make a comparison to the strong-collision approximation, where the solution is given by Eq. (31).

In the myocardium of the heart the volume fraction η corresponds to the so-called regional blood volume (RBV $\approx 10\div 20\%$). The capillaries have a diameter of about 10 μm and the surrounding tissue has a diffusion coefficient of about 1 μm^2/ms [11]. The frequency shift $\delta\omega$ is proportional to the susceptibility difference $\Delta\chi$ which is influenced by the blood oxygenation level or the concentration of the intravasal contrast agent and takes values in the order of $\Delta\chi\approx 10^{-7}\div 10^{-8}$ [11]. To compare the results for cylinders and spheres we choose the same parameters for the case of spheres, since typical parameters of magnetically labeled cells are in the same range [15,34].

Table I shows the geometrical and physical parameters, for which calculations have been performed numerically, together with the number of mesh points, for which convergence was verified. The values for the inner and outer radii were chosen such that the volume fraction η (14, 17) is equal to 0.2, both for cylinders and spheres. In the solution of the boundary-value problem for $D=0$, a finite line broadening $\gamma=1$ s^{-1} was introduced both for cylinders and spheres. In the solution of the initial-value problem of the Bloch-Torrey

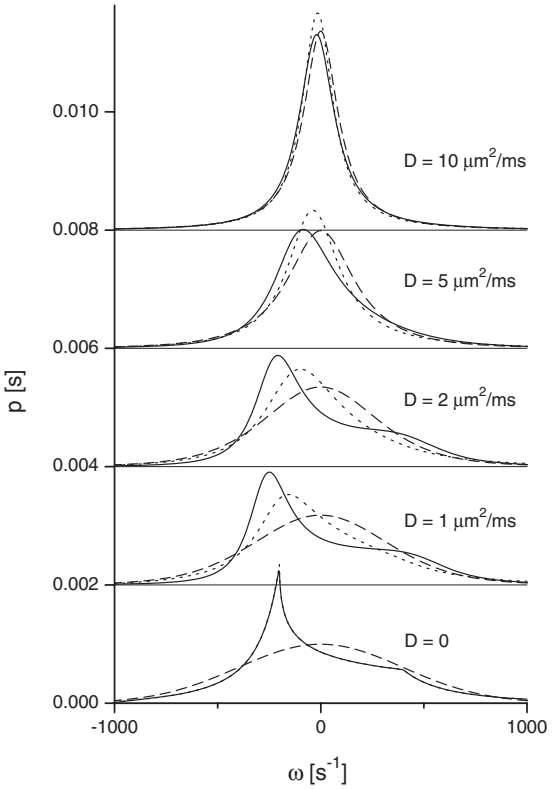

FIG. 5. Frequency distribution $p(\omega)$ in the case of spheres for $R_1=5$ μm, $R_2=8.55$ μm, $\delta\omega=1000$ s^{-1}, and various values of the diffusion coefficient $D=0$, 1, 2, 5, and 10 $\mu m^2/ms$ (from bottom to top). Solid line: full numerical solution, dashed line: Gaussian approximation, and dotted line: strong-collision approximation.

equation, sufficient accuracy was achieved when the parameter ϵ in Eq. (58) was chosen to be 10^{-3}. All calculations were performed with double precision. For the initial-value problem we verified that the lowest eigenvalue $E^{(0)}$ of the matrix $-\mathbf{\Delta}$ in Eq. (50) fulfills $|E^{(0)}|t_{max} \ll 1$, where t_{max} is the time span for which the solution was calculated.

With increasing values of D, the line broadening increases, the mesh can be made coarser, and the computing time is significantly reduced, as not only the matrix dimension becomes smaller, but the step size (58) can also be made larger as $\|\mathbf{\Delta}\|$ becomes smaller. For $D=1$ $\mu m^2/ms$, the solution of the initial-value problem was done within minutes, so for larger D we did not try to find the minimum number of mesh points. Actually, for matrix dimensions $(41\times51)\times(41\times51)$ one could even employ methods for full matrices.

In Fig. 2, the average magnetization M is shown as function of time t in the case of cylinders for the parameters specified in Table I. The full numerical solution (solid line) is compared with the solution in the Gaussian approximation (dashed line) and the strong-collision approximation (dotted line).

The Bloch-Torrey equation and the diffusion equation were solved in time domain. For the strong-collision approximation, the expression (31) was Fourier-transformed numerically.

For $D=0$, the average magnetization exhibits a square-exponential decay in the short-time limit. However, the function becomes negative for intermediate times. In the long-time limit, the average magnetization shows an oscillatory behavior with slowly decaying amplitude. In contrast, the Gaussian approximation shows a square exponential decay in the whole time range, as seen from the analytical expression (25). As expected, the Gaussian approximation is accurate in the short-time limit, but totally fails for intermediate and large times. The strong-collision approximation becomes exact for $D=0$, as $p(\omega)$ goes over into the classical density of states (13). There is no visible difference between the full numerical solution and the solution in the strong-collision approximation which means that the numerical accuracy is sufficient.

With increasing values of the diffusion coefficient, up to about $D=2$ $\mu m^2/ms$, the minimum of the exact solution becomes sharper and occurs at shorter times. For larger values of D the minimum becomes less pronounced, it shifts to the right. Eventually, for large values of the diffusion coefficient, the minimum completely disappears and $M(t)$ decreases monotonously.

In the Gaussian approximation, the average magnetization is always positive, as can be seen from expression (22). The decay becomes slower with increasing values of D and goes over from square exponential to linear exponential. Only in the limit of large D, there is reasonable agreement between Gaussian approximation and exact solution in the whole time range. The strong-collision approximation qualitatively behaves like the exact solution, but the minimum of the signals for intermediate D is much less pronounced. In fact, starting from $D \geq 1$ $\mu m^2/ms$, the strong-collision approximation is closer to the Gaussian approximation than to the exact solution and lies between the exact solution and the Gaussian approximation for intermediate D. For large D, starting somewhat below $D=5$ $\mu m^2/ms$, the Gaussian approximation is closer to the exact solution than is the strong-collision approximation.

The corresponding frequency distribution is shown in Fig. 3. Here, the Bloch-Torrey equation was solved in frequency domain and we verified that the solution is equivalent to that of Fig. 2 by Fourier transform. For the diffusion equation, the solution has been calculated in time domain and then Fourier-transformed numerically. The solution in the strong-collision approximation is given by the analytical expressions (31).

As $M(t)$ is real and symmetric, the function $p(\omega)$ is symmetric. For $D=0$, the full numerical solution and the strong-collision approximation coincide, except for the very neighborhood of a maximum. The reason is that for the strong-collision approximation which becomes exact for $D=0$ no numerical lifetime broadening γ was introduced. These peaks are not at all found in the Gaussian approximation, where the frequency distribution is a Gaussian (25).

For intermediate values of the diffusion coefficient, $D=1\ldots2$ $\mu m^2/ms$, the exact solution still exhibits two pronounced maxima. These maxima are somewhat flattened, but their distance is larger than for $D=0$. Thus, in contrast to the strong-collision approximation, the behavior of the exact solution cannot be explained by a mere increase of the damping rate. For the strong-collision approximation, the minimum disappears much faster than for the exact solution;

starting at about $D=2\ \mu m^2/ms$, the two peaks have mold to a single maximum and the strong-collision much closer resembles the Gaussian approximation than the exact solution.

For large D, the minimum also disappears for the exact solution, and both the Gaussian approximation and the strong-collision approximation slowly converge towards the exact solution. In the limit $D\to\infty$, the frequency distribution goes over into a Lorentzian.

The functions $|M(t)|$ and $p(\omega)$ in the case of spheres are shown in Figs. 4 and 5, respectively. For the exact solution and the strong-collision approximation, the average magnetization is complex and, therefore, the frequency distribution is not symmetric, in contrast to the Gaussian approximation. Otherwise, the same phenomena are observed as for cylinders. In the Gaussian approximation, the density of states for $D=0$ is a Gaussian and goes over into a Lorentzian in the limit $D\to\infty$. The Gaussian approximation becomes exact for $D\to\infty$, but totally fails for $D\to 0$. The strong-collision approximation is exact in both limits, but for $D\to\infty$, the convergence is slower than for the Gaussian approximation. For intermediate values of the diffusion coefficient, none of the approximations closely resemble the exact solution.

The results in this section where obtained using specific lengths, frequency shifts, and diffusion coefficients. It is also interesting to look for non-dimensional solutions of the Bloch-Torrey equation, as was done by Hürlimann in another context [17]. As the geometry (radii R_1 and R_2) is basically fixed, the free parameters which can be changed in an experiment are $\delta\omega$ and D (by variation of the field strength or the temperature). As discussed at the beginning of Sec. III, there are two choices for introducing dimensionless quantities. A time scale can either be defined by the characteristic dephasing time $\tau_1=1/\delta\omega$ or by the characteristic diffusion time $\tau_2=R_1^2/D$. Then, for a given geometry, a catalog of solutions can be produced depending only on the dimensionless time t/τ_1 (or t/τ_2) and the dimensionless parameter $\tau_2/\tau_1=R_1^2\delta\omega/D$.

V. SUMMARY AND CONCLUSIONS

In this paper, we developed a numerical method to solve the Bloch-Torrey equation in time and frequency domain using finite differences. Especially the solution in time domain is highly efficient, flexible, and easy to use.

As an example, we considered the important cases of cylinders and spheres, commonly used as idealizations for blood-filled capillaries and magnetically labeled cells. The results were compared with the Gaussian approximation and the strong-collision approximation. The Gaussian approximation becomes exact in the short-time limit and in the limit of large diffusion coefficients; otherwise it leads the wrong results, even qualitatively. The strong-collision approximation becomes exact both in the limit of small and large diffusion coefficients, but in the latter case the convergence is slower than for the Gaussian approximation. For intermediate values of the diffusion coefficient, the strong-collision only qualitatively resembles the exact solution. Thus a full numerical solution is the only way to study the magnetization decay in the intermediate regime.

ACKNOWLEDGMENTS

This work was supported by the Deutsche Forschungsgemeinschaft—Sonderforschungsbereich 688 "Mechanismen und Bildgebung von Zell-Zell-Wechselwirkungen im kardiovaskulären System." C.H.Z. thanks the Berufsverband Deutscher Internisten, Wiesbaden, Germany, for support.

[1] A. Krogh, J. Physiol. (London) **52**, 409 (1919).
[2] H. C. Torrey, Phys. Rev. **104**, 563 (1956).
[3] D. S. Grebenkov, Rev. Mod. Phys. **79**, 1077 (2007).
[4] S. D. Stoller, W. Happer, and F. J. Dyson, Phys. Rev. A **44**, 7459 (1991).
[5] P. Le Doussal and P. N. Sen, Phys. Rev. B **46**, 3465 (1992).
[6] V. M. Kenkre, E. Fukushima, and D. Sheltraw, J. Magn. Reson. **128**, 62 (1997).
[7] P. Gillis and S. H. Koenig, Magn. Reson. Med. **5**, 323 (1987).
[8] D. A. Yablonskiy and E. M. Haacke, Magn. Reson. Med. **32**, 749 (1994).
[9] R. P. Kennan, J. Zhong, and J. C. Gore, Magn. Reson. Med. **31**, 9 (1994).
[10] W. R. Bauer, W. Nadler, M. Bock, L. R. Schad, C. Wacker, A. Hartlep, and G. Ertl, Phys. Rev. Lett. **83**, 4215 (1999).
[11] W. R. Bauer, W. Nadler, M. Bock, L. R. Schad, C. Wacker, A. Hartlep, and G. Ertl, Magn. Reson. Med. **41**, 51 (1999).
[12] A. L. Sukstanskii and D. A. Yablonskiy, J. Magn. Reson. **163**, 236 (2003).
[13] A. L. Sukstanskii and D. A. Yablonskiy, J. Magn. Reson. **167**, 56 (2004).
[14] W. R. Bauer, C. H. Ziener, and P. M. Jakob, Phys. Rev. A **71**, 053412 (2005).
[15] C. H. Ziener, T. Kampf, G. Melkus, V. Herold, T. Weber, G. Reents, P. M. Jakob, and W. R. Bauer, Phys. Rev. E **76**, 031915 (2007).
[16] C. H. Ziener, T. Kampf, G. Melkus, P. M. Jakob, and W. R. Bauer, J. Magn. Reson. **184**, 169 (2007).
[17] M. D. Hürlimann, J. Magn. Reson. **131**, 232 (1998).
[18] M. Hürlimann, K. Helmer, and C. Sotak, Magn. Reson. Imaging **16**, 535 (1998).
[19] E. M. Haacke, R. W. Brown, M. R. Thompson, and R. Venkatesan, *Magnetic Resonance Imaging: Physical Principles and Sequence Design* (Wiley, New York, 1999).
[20] R. Freeman and H. D. W. Hill, J. Magn. Reson. **4**, 366 (1971).
[21] M. L. Gyngell, J. Magn. Reson. **81**, 474 (1989).
[22] K. Scheffler and J. Hennig, Magn. Reson. Med. **49**, 395 (2003).
[23] H. Y. Carr and E. M. Purcell, Phys. Rev. **94**, 630 (1954).
[24] J. Stepisnik, Physica B **270**, 110 (1999).
[25] P. W. Anderson and P. R. Weiss, Rev. Mod. Phys. **25**, 269 (1953).
[26] D. C. Douglass and D. W. McCall, J. Phys. Chem. **62**, 1102 (1958).

[27] C. H. Neuman, J. Chem. Phys. **60**, 4508 (1974).
[28] C. H. Ziener, T. Kampf, V. Herold, P. M. Jakob, W. R. Bauer, and W. Nadler, J. Chem. Phys. **129**, 014507 (2008).
[29] C. H. Ziener, W. R. Bauer, G. Melkus, T. Weber, V. Herold, and P. M. Jakob, Magn. Reson. Imaging **24**, 1341 (2006).
[30] W. H. Press, S. A. Teukolsky, W. T. Vetterling, and B. P. Flannery, *Numerical Recipes in FORTRAN—The Art of Scientific Computing*, 2nd ed. (Cambridge University Press, Cambridge, England, 1992).
[31] S. Glutsch, *Excitons in Low-Dimensional Semiconductors: Theory, Numerical Methods, Applications* (Springer, Berlin, 2004).
[32] W. F. Ames, *Numerical Methods for Partial Differential Equations* (Academic Press, Boston, 1992).
[33] R. D. Richtmyer and K. W. Morton, *Difference Methods for Initial-Value Problems* (Krieger, Malabar, FL, 1994).
[34] C. H. Ziener, W. R. Bauer, and P. M. Jakob, Magn. Reson. Med. **54**, 702 (2005).